Journal of Electrical and Computer Engineering Innovations
(JECEI)
Journal homepage: http://www.jecei.sru.ac.ir

Research paper

Nonlinear Filter-Based Estimation of Wheel-Rail Contact Forces and Related Considerations using Inertial Measurement Unit

M. Moradi, R. Havangi *

Faculty of Electrica l Engineering and Computer, University of Birjand, Birjand, Iran.

Article Info

Article History:
Received 08 September 2024
Reviewed 28 November 2024
Revised 11 January 2025
Accepted 15 January 2025

Keywords:
Adhesion coefficient traction system
Wheel slip
Nonlinear filter
Vehicle dynamics

Corresponding Author's Email Address:
Havangi@Birjand.ac.ir

Abstract

Background and Objectives: Rail vehicle dynamics are significantly influenced by the forces at the wheel-rail contact interface, particularly the wheel-rail adhesion force, which is critical for effective braking and acceleration. Continuous monitoring of this force is essential to prevent infrastructure damage and enhance transportation efficiency. Given the challenges of directly measuring adhesion force, alternative methods using state observers have gained prominence. The choice of model and estimator efficacy are vital for accurate variable estimation.
Methods: In this study, the dynamics of the wheelset is simulated in the presence of irregularities that can be encountered in the railroad. Estimation of wheel-rail adhesion force is done indirectly by nonlinear filters as estimators and their accuracies in the estimation are compared to identify the better one. Meanwhile, inertial sensors (accelerometer and gyroscope) outputs are used as measuring matrix and employed to simulate actual situation and evaluate the estimators' performances. The proposed approach is implemented in MATLAB to assess the accuracy and effectiveness of these estimators in determining states and variables.
Results: The proposed method effectively utilizes longitudinal, lateral, and torsional dynamics to estimate wheel-rail adhesion force across varying conditions. Experimental results demonstrate high precision, rapid convergence, and low error rates in the estimations.
Conclusion: In this study, the identification of the wheel and rail contact conditions is carried out by analyzing the dynamic characteristics of the railway wheelset. The results of proposed method can lead to decreasing wheel deterioration and operational costs, minimizing high creep levels, maximizing the use of already-existing adhesion, and improving the frequency of service. It is worth noting that the proposed method is beneficial for both conventional railway transport and automated driverless trains.

Introduction

Modeling wheel-rail interactions is inherently complex, particularly when diverse track conditions are considered. As model complexity increases, the computational load also rises, leading to extended response times. Consequently, to maintain computational efficiency, it is essential to focus on the most significant and influential components that impact the wheel-rail forces. The tangential forces at the wheel-rail interface are the key components in the wheel-and-rail interface and are caused by wheel and rail relative motion. In fact, the available evidence suggests that the motion is defined by a gradual sliding phenomenon at the contact surface known as creepage. The forces caused by creepage are denoted as creep forces, and they control how well a rail vehicle accelerates and brakes. Adhesion is determined as the ratio of the tangential frictional force between the wheel and rail to the load of the wheel. The friction

coefficient is defined as the ratio between the friction force and the normal force at the contact surface [1]. The friction coefficient always limits the adhesion coefficient [2]. As a result, there may be differences between the adhesion and friction coefficients.

In [3] the importance of friction in determining wheel and rail adhesion is discussed. Estimating adhesion in the wheel and rail contact region is a complex procedure because it depends on a number of operational variables, including the operational mechanism of rail self-cleaning, axle load distributions, track irregularities, and processes occur at the wheel and rail nonlinear contact interface. Effective and continuous monitoring of the adhesion coefficient is necessary for estimating the maximum adhesion force and preserving a satisfactory braking and acceleration performance, but measuring the adhesion coefficient with a conventional physical sensor is difficult [4]. The adhesion coefficient is highly dependent on any materials that are present at the wheel and rail interface, including water [5], leaves [6], [7], snow, oil, and grease. The wheel and rail adhesion characteristics have different behaviour under large sliding conditions and as the slip ratio rises, the adhesion coefficient keeps rising after it reaches the saturation point instead of decreasing [8]. Numerous researchers attempted to solve the adhesion problem, and various approaches, including statistical, genetic, and mathematical control theory, were put forth and applied [9], [10]. Two key elements influencing the railway surfaces are train velocity and contact area temperature [11]. The maximum adhesion coefficient is reached at higher values of both the adhesion coefficient and the slip velocity.

As such, determining the adhesion level is a crucial task for a rail vehicle to operate properly. In [12], a novel method for figuring out the adhesion coefficient between the wheel and rail was presented. Furthermore, a different adhesion control method based on tracking the adhesion status between the wheel and rail is presented in another research paper [13]. Traction power in trains can be efficiently utilized when optimal adhesion control is achieved [14], [15]. It is noteworthy to mention that in order to prevent wheel slippage or slide, the creep velocity of the train within the stable region must be limited in accordance with the changes seen in the adhesion coefficient characteristic curve. In [16] re-adhesion control is used to bring the trains back to the stable region by quickly identifying instances of wheel slide and adjusting the torque precisely. The correct selection of the initial model by considering the most important factors related to adhesion force and the selection of an estimator that is compatible with the structure of the system under study can create a more reliable and accurate output. Due to the nonlinear nature of the adhesion coefficient, the use of nonlinear types of Kalman filters has been of great interest. An innovative method that estimates the wheel and rail states using the Kalman-Bucy filter (KBF) approach is suggested in [17] to predict the wheel and rail wear, regions of adhesion variations or low adhesion, and the development of rolling contact fatigue. Additionally, the lateral creep force is detected for the purpose of determining the local adhesion condition using the KBF [18]. In [19], a model-based approach utilizing Extended Kalman Filter (EKF) is presented to estimate the adhesion force in the wheel and rail contact surface. But the strategy is not evaluated on every track circumstance. In [20], an EKF based estimation method was proposed for estimating the slip, creep force, and friction coefficient between the wheel and rail surface using the induction motor current, stator voltage, and speed. Using multi-rate EKF state identification is an alternate method for detecting slip velocity. This method determines the traction motor load torque accurately by combining the EKF method with the multi-rate technique. Faster slip detection, enhanced dependability, and better traction performance are the benefits of this approach [21].

The adhesion coefficient was found as a function of slip velocity in [22]. To estimate the slip velocity, the measured wheel velocity was fed into the EKF. In order to attain the best outcome, various EKF configurations were examined and adjusted in this study using system and measurement noise covariance matrices. Real-time wheel-rail contact force and moment estimation based on an EKF estimator under typical driving circumstances is represented by the researchers in [23]. EKF uses a Jacobian matrix in states estimation which is an error-prone process [24]. To overcome these problems, an unscented transformation proposed in [25]. A model-based approach using Unscented Kalman Filter (UKF) is proposed in [26] for estimation of friction coefficient, creep force, and creepage. The UKF faces challenges with numerical stability when applied to high-dimensional systems due to the fact that the central stem (mean) of the sigma points carries a heavier weight, often negative, in such systems. Nevertheless, estimators appear to be unreliable in certain crucial track conditions, so more work is required to more effectively monitor these wheel-rail parameters in real time. Meanwhile, after reviewing the literature on railway wheelset dynamics condition monitoring, it is found that more effort and improvement need to be done to solve the issue of analyzing wheelset conditions and updating them to the desired situation in order to meet the global transportation vehicle expectations of extremely fast, high comfort, increased safety, and cost-effectiveness.

For optimal operation, the Kalman filter requires a system model. Also, mathematical models of important processes are necessary for the methodical process of

adhesion estimation. In addition to the mentioned methods, adhesion condition was estimated [27] and wheel-rail contact force was predicted [28] using the artificial neural network approach. These methods, however, ignore a number of important factors, including changes in the wheel and rail profiles and friction levels. Use of the traditional wheel-rail contact algorithms [29], which are employed in multi-body software packages and yield accurate results, is preferable in this situation. Nevertheless, the low computational speed of the classical contact models makes them unsuitable for real-time implementation. The fast approximation model seems to offer satisfactory precision in order to achieve real-time simulation by fulfilling the criteria specified in the literature [30]. However, it is not capable of taking contact profile changes into account and requires user-defined coefficients in models.

The aim of this research is to assess the adhesion force and slip in the contact region of the wheel and rail with accuracy by using nonlinear filters approach. It is worth noting that in this process EKF and UKF are employed for estimation as nonlinear filters. The main goal of this experiment is to determine, whether employing UKF in the system allows to achieve better results in respect to the EKF. Analysis of the measured inertial sensors values is used in estimation process. To evaluate the observer's performance, a dynamic model is constructed, comprising lateral, longitudinal, and yaw dynamics of the wheelset. In summary, the manuscript introduces a novel, comprehensive approach by employing nonlinear filtering that integrates Inertial Measurement Units (IMUs) data to estimate wheel-rail contact forces in real-time. The Polach model is utilized to explain the wheel-rail contact conditions. The rest of this research is organized into four parts. First, the details of lateral, longitudinal and yaw dynamical model of the wheelset are explained. Then, the process of estimator design is outlined. This is followed by an in-depth discussion of the experimental results. Finally, the conclusion is presented.

Lateral, Longitudinal and Yaw Dynamical Model of the Wheelset

If the rail is considered to be rigid, the wheelset has three degrees of freedom namely longitudinal, lateral, and yaw motions. Compared to longitudinal displacement, yaw and lateral displacement are very small but they have the key role in stability and ride comfort of the vehicle. The interaction between the wheel and rail contact area influences the dynamic performance of the rail vehicle. In order to design dynamic control systems and monitor the situation more efficiently, it is very important to know the nature of the contact force. Also, to prevent the wheel from slipping during traction and sliding during braking, it is important to know the adhesion not only in normal operating conditions but also during traction and braking. Estimation of adhesion coefficient, slip ratio, and lateral dynamics of rail vehicle in traction and braking modes are essential for travel safety and passenger comfort. Wheel-rail adhesion mechanism is shown in Fig. 1. A more complex model leads to an increase in computational load and an increase in response time. As a result, in order to maintain computational efficiency, it is necessary to focus on the most important and influential components affecting the wheel and rail forces in the estimation process. This approach allows for a more balanced trade-off between model accuracy and processing speed and facilitates practical real-time applications.

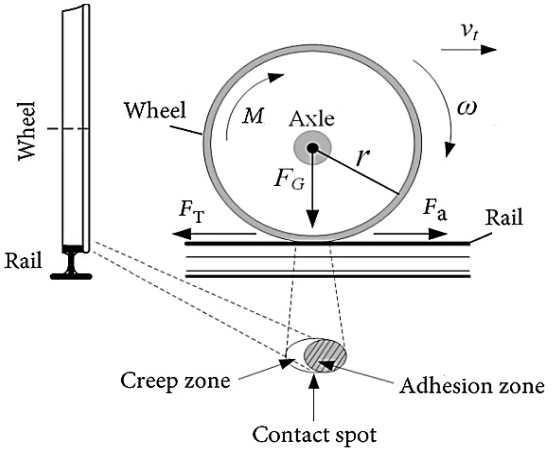

Fig. 1: Wheel-rail adhesion mechanism.

Estimating the dynamics of the wheelset is a complex process because the wheel and rail interface is an open loop system with variable external conditions. A novel model-based methodology has been devised in this study to estimate the most important dynamics of the wheelset in various contact conditions. Since the Kalman filter (KF) is not suitable estimator for the nonlinear contact system of wheel and rail, therefore, EKF is employed to estimate the adhesion coefficient, slip ratio, and lateral dynamics of the wheelset. The system utilized in this research is shown in Fig. 2, which consists of two wheels and an axle.

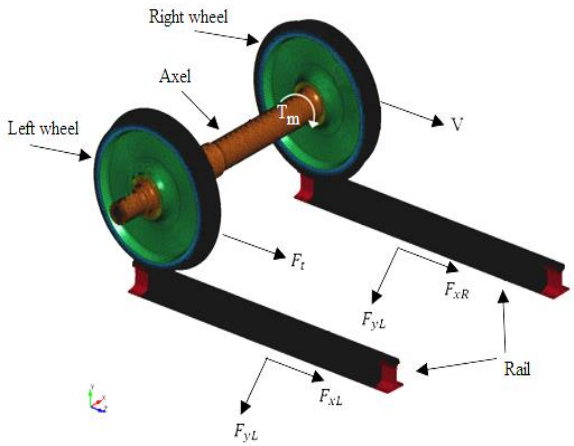

Fig. 2: Three-dimensional wheel-rail system model.

There is a direct correlation between the lateral and yaw dynamics and track irregularities. The left and right wheels' linear speeds will differ if the wheelset moves sideways from its initial position. These speeds are obtained from the following relations:

$$V_{Rw} = \omega_R.[r - \kappa_w(y - y_d)] \quad (1)$$

$$V_{Lw} = \omega_L.[r + \kappa_w(y - y_d)] \quad (2)$$

where V_{Rw} and V_{Lw} are longitudinal velocity of the right and left wheels, ω_R and ω_L are angular velocity of the right and left wheels, r is wheel radius, $\kappa_w$is wheel conicity, y is lateral movement, and y_d is track irregularities in lateral direction.

The wheelset's dynamic characteristics are also influenced by the creep forces that arise in the contact zones between the wheel and rail. These creep forces, which can be classified as longitudinal creepage (ξ_x) and lateral creepge (ξ_y) depending on the direction of movement, are brought on by the creeps that arise from the wheels' relative speed to the rail. The creepage of both wheels in the wheelset in the lateral and longitudinal directions are displayed in equations (3)-(5).

$$\xi_{Rx} = \frac{r\omega_R - V}{V} - [\frac{S\dot{\psi}}{V} + \frac{\kappa_w(y - y_d)}{r}] \quad (3)$$

$$\xi_{Lx} = \frac{r\omega_L - V}{V} + \frac{S\dot{\psi}}{V} + \frac{\kappa_w(y - y_d)}{r} \quad (4)$$

$$\xi_y = \xi_{Ly} = \xi_{Ry} = \frac{\dot{y}}{V} - \psi \quad (5)$$

where ξ_{Rx} and ξ_{Lx} are longitudinal creepage of the right and left wheels, ξ_{Ry} and ξ_{Ly} are lateral creepage of the right and left wheels, S is half gauge of track, $\dot{\psi}$ is yaw rate, $\dot{y}$ is lateral velocity, ψ is yaw angle, and V is train longitudinal velocity.

In equations (3) and (4), the expressions $\frac{r\omega_R - V}{V}$ and $\frac{r\omega_L - V}{V}$ do not include dynamics related to y and ψ, therefore can be ignored to simplify longitudinal creepage equations. In addition, the dynamics consist of lateral displacement and yaw rate are sufficient in identifying alterations in the wheel-rail contact conditions. The simplified longitudinal creepage equations are as follows:

$$\xi_{Rx} = -\frac{S\dot{\psi}}{V} - \frac{\kappa_w(y - y_d)}{r} \quad (6)$$

$$\xi_{Lx} = \frac{S\dot{\psi}}{V} + \frac{\kappa_w(y - y_d)}{r} \quad (7)$$

The total slip ξ_j is a combination of longitudinal ξ_{jx} and lateral ξ_{jy} slips and obtained from the following equation:

$$\xi_j = \sqrt{\xi_{jx}^2 + \xi_{jy}^2} \qquad j\text{=L or R} \quad (8)$$

The creep force F_j can be expressed as a nonlinear function of the slip, which is determined by utilizing the given equation in (9).

$$F_j = \mu_j F_{Nj} \qquad j\text{=L or R} \quad (9)$$

In normal conditions and for small amounts of creepage (microslip), F_j changes linearly with creepage. As the sliding speed increases, the creep force changes nonlinearly and reaches the maximum value (saturation), and if the increase in sliding speed continues, it begins a downward trend. In general, to describe wheelset stable and unstable behaviors, the adhesion-slip curves can be divided into three areas. The initial section displays a nearly linear pattern, followed by a nonlinear segment known as the high slip ratio region, and concluding with a negative slope indicating the unstable zone of the curve. Fig. 3 shows the details.

The nonlinear region is strongly influenced by factors such as pollution and weather and it results in large and uncertain changes in the creep force. The analysis of contact force distribution in both the longitudinal and lateral orientations was thoroughly studied in [31]. These forces can be calculated using equation (10).

$$F_{ji} = F_j \frac{\xi_{ji}}{\xi_j} \qquad j\text{=L or R} \quad \& \quad i\text{= } x \text{ or } y \quad (10)$$

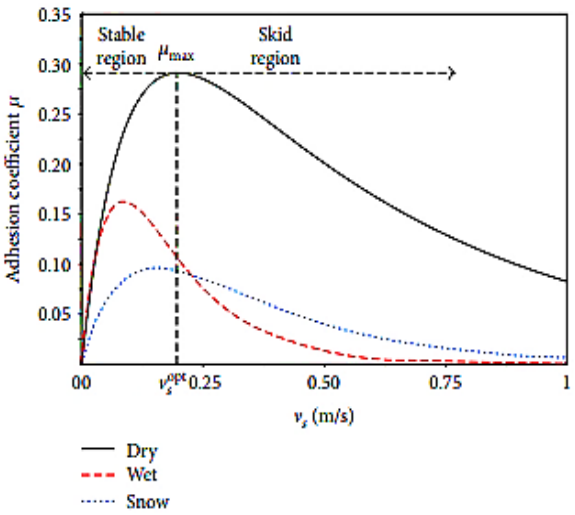

Fig. 3: Adhesion curves [9].

An entire wheelset model encompasses every aspect of the interactions between wheels and rails, facilitating the analysis of wheelset dynamics. The given equations below represent the motion of the wheelset at any location along the creep curve for yaw, rotational, torsional, lateral, and longitudinal dynamics.

$$\ddot{x} = \frac{F_{Rx} + F_{Lx}}{M_t} \quad (11)$$

$$\ddot{y} = \frac{-F_{Ry} - F_{Ly} + F_C}{m_w} \quad (12)$$

$$\ddot{\psi} = \frac{F_{Rx}S - F_{Lx}S - K_w\psi}{J_w} \quad (13)$$

$$T_s = t_s\theta_s + C_{vis}(\omega_R - \omega_L) \quad (14)$$

$$\theta_s = \int(\omega_R - \omega_L)dt \quad (15)$$

$$\dot{\omega}_L = \frac{T_s - T_L}{J_L} \quad (16)$$

$$\dot{\omega}_R = \frac{T_m - T_s - T_R}{J_R} \quad (17)$$

where F_{Rx} and F_{Lx} ara right and left wheel creep forces in longitudinal direction, M_t is rail vehicle mass, F_{Ry} and F_{Ly} ara right and left wheel creep forces in lateral direction, m_w is total weight of wheel with induction motor, F_c is centrifugal force, K_w is yaw stiffness, J_w is wheelset moment of inertia, T_s is torsional torque, t_s is torsional Stiffness of axle, θ_s is twist angle, C_{vis} is viscous material damping of the shaft, T_R and T_L are right and left wheel tractive torques, T_m is motor torque, and J_R and J_L are inertias of right and Left wheel.

In equation (12) F_C is considered when the wheels travel along a crooked railroad track. In equation (14) C_{vis} can be disregarded because it is typically very small. In the above equations, F_{xR}, F_{xL}, F_{yR}, F_{yL}, T_m, T_L, and T_R are defined as follows:

$$F_{Rx} = \frac{F_R}{\xi_R}\left[\left[\frac{r\omega_R - V}{V} - \left[\frac{S\dot{\psi}}{V} + \frac{\kappa_w(y - y_d)}{r}\right]\right]\right] \quad (18)$$

$$F_{Lx} = \frac{F_L}{\xi_L}\left[\frac{r\omega_L - V}{V} + \frac{S\dot{\psi}}{V} + \frac{\kappa_w(y - y_d)}{r}\right] \quad (19)$$

$$F_{Ry} = \frac{F_R}{\xi_R}\left[\frac{\dot{y}}{V} - \psi\right] \quad (20)$$

$$F_{Ly} = \frac{F_L}{\xi_L}\left[\frac{\dot{y}}{V} - \psi\right] \quad (21)$$

$$T_m = \mu M_t g r \quad (22)$$

$$T_L = r F_{Lx} \quad (23)$$

$$T_R = r F_{Rx} \quad (24)$$

As can be seen from the above equations, the dynamics of the wheelset are complex and all the movements of the wheelset are interdependent. Due to the powerful interactions exist between different wheel movements in lateral and longitudinal directions, it is of great importance to utilize a general model that encompasses all the motions associated with contact forces in the investigation of the wheelset dynamics. Wheels directly interact with the rail, as a result, any alterations in contact conditions will affect the wheelset dynamics.

This study uses a model-based methodology to estimate the variables related to wheel-rail contact. Model-based estimation utilizes the system's information through a mathematical framework and measured responses to the input to estimate the state variables of the system in real time. For practical purposes, the estimator design should be as simple as possible while taking into account the wheelset dynamics that are associated with the contact conditions. Therefore, the wheelset model [32] is simplified first.

$$\ddot{y} = -\frac{F_R}{m_w \xi_R}\left[\frac{\dot{y}}{V} - \psi\right] - \frac{F_L}{m_w \xi_L}\left[\frac{\dot{y}}{V} - \psi\right] \quad (25)$$

$$\ddot{\psi} = \frac{F_R}{J_w \xi_R}\left[-\frac{S\dot{\psi}}{V} - \frac{\kappa_w(y - y_t)}{r}\right]S - \frac{F_L}{J_w \xi_L}\left[\frac{S\dot{\psi}}{V} + \frac{\kappa_w(y - y_t)}{r}\right]S - \frac{K_w \psi}{J_w} \quad (26)$$

The simplified model has numerous benefits. The primary advantage lies in the straightforward estimator design with the fewest number of states, which enables the fast convergence of the estimator. In addition, in the simplified model, no input torque is required for the estimator, and yaw and lateral dynamics are affected by track disturbances. Since the relation between the adhesion coefficient μ and slip ξ is nonlinear, assuming that the wheels on both sides, i.e. the left and right, have the same contact conditions, first, equations (25) and (26) are arranged and the lateral and yaw dynamic models of the wheelset are derived.

$$\ddot{y} = -\frac{1}{V m_w}\left(\frac{F_R}{\xi_R} + \frac{F_L}{\xi_L}\right)\dot{y} + \frac{1}{m_w}\left(\frac{F_R}{\xi_R} + \frac{F_L}{\xi_L}\right)\psi \quad (27)$$

$$\ddot{\psi} = -\frac{S^2}{V J_w}\left(\frac{F_R}{\xi_R} + \frac{F_L}{\xi_L}\right)\dot{\psi} - \frac{S}{r J_w}\kappa_w\left(\frac{F_R}{\xi_R} + \frac{F_L}{\xi_L}\right)y + \frac{S}{r J_w}\kappa_w\left(\frac{F_R}{\xi_R} + \frac{F_L}{\xi_L}\right)y_t - \frac{K_w}{J_w}\psi \quad (28)$$

In the second step, by considering the equalities in (29) and replacing them in equations (27) and (28), equations (30) and (31) are obtained.

$$F_R = F_L = F_a \quad \& \quad \xi_L = \xi_R = \xi \quad (29)$$

$$\ddot{y} = -\frac{2F_a}{\xi m_w}\left(\frac{\dot{y}}{V} - \psi\right) \quad (30)$$

$$\ddot{\psi} = -\frac{2F_a S^2}{\xi V J_w}\dot{\psi} - \frac{2F_a S}{\xi r J_w}\kappa_w(y - y_t) - \frac{K_w}{J_w}\psi \quad (31)$$

Other process variables are defined as follows:

$$\xi = \sqrt{\left(\frac{\kappa_w(y - y_d)}{r} + \frac{S\dot{\psi}}{V}\right)^2 + \left(\frac{\dot{y}}{V} - \psi\right)^2} \quad (32)$$

$$\mu = \mu_0((1 - D)e^{-B\xi V} + D) \quad (33)$$

$$F_a = \frac{2F_N\mu}{\pi}\left(\frac{k_A\varepsilon}{1 + (k_A\varepsilon)^2} + \arctan(k_S\varepsilon)\right) \quad (34)$$

$$\varepsilon = \frac{2\pi a^2 bc}{3F_N\mu_{k-1}}\xi_{k-1} \quad (35)$$

where F_N is the normal force, D and B are reduction factors associated with distinct friction coefficients, G is shear module, a and b are the semi-axis length of the ellipse in contact zone, and C_{11} is the Kalker coefficient.

In the following, the design of the estimator is discussed.

Nonlinear Filter-Based Estimation of Wheel-Rail Contact Forces

The details of the filters used for estimation of wheel-rail lateral dynamics can be found in the following subsections. The discrete-time nonlinear model is presented as follows:

$$\begin{aligned} x_{k+1} &= f(x_k, u_k) + w_k \\ z_k &= h(x_k) + v_k \end{aligned} \quad (36)$$

where $f(.)$ represents the dynamics of wheelset, h(.) is the relationship between the observation z_k and the state

vector x_k, $u_k$refers to the input vector, while w_k and v_k represent the vectors of noise that affect the process and measurement respectively. The state variables used to create the EKF algorithm process matrix include lateral velocity ($\dot{y}$), yaw rate ($\dot{\psi}$), slip ratio (ξ), friction coefficient (μ), and adhesion force (F_a). Besides, lateral acceleration ($\ddot{y}$) and yaw rate are considered to create the measurement matrix.

$$x = \begin{bmatrix} \dot{y} & \dot{\psi} & \xi & \mu & F_a \end{bmatrix}^T$$
$$z = [\ddot{y} \quad \dot{\psi}] \tag{37}$$

To design nonlinear filter, the model used for estimation must also be discrete. Therefore, equations (30)-(34) should be discretized, the result of which is given below.

$$\dot{y}_k = \dot{y}_{k-1} - \frac{2\tau F_{ak-1}}{\xi_{k-1} m_w}\left[\frac{\dot{y}_{k-1}}{V} - \psi\right] \tag{38}$$

$$\dot{\psi}_k = \dot{\psi}_{k-1} - \frac{2\tau S F_{ak-1}}{\xi_{k-1} J_w}\left[\frac{\kappa_w (y - y_d)}{r} + \frac{S\dot{\psi}_{k-1}}{V}\right] - \frac{K_w \psi}{J_w} \tag{39}$$

$$\xi_k = \sqrt{\left(\frac{\kappa(y-y_d)}{r} + \frac{S\dot{\psi}_{k-1}}{V}\right)^2 + \left(\frac{\dot{y}_{k-1}}{V} - \psi\right)^2} \tag{40}$$

$$\mu_k = \mu_0\left((1-D)e^{-B\xi_{k-1}V} + D\right) \tag{41}$$

$$F_{ak} = \frac{2F_N \mu_{k-1}}{\pi}\left(\frac{k_A \varepsilon}{1+(k_A\varepsilon)^2} + \arctan(k_S \varepsilon)\right) \tag{42}$$

The components of the measurement matrix are as follows:

$$\ddot{y}_k = -\frac{2F_a}{\xi m_w}\left(\frac{\dot{y}_{k-1}}{V} - \psi\right) \tag{43}$$

The second component of the measurement matrix, i.e. $\dot{\psi}$, is obtained as equation (39).

A. Extended Kalman Filter

The EKF is an improved version of the conventional KF designed to handle nonlinear systems. The primary objective of this research is to identify the best estimation for the state vector of the wheelset. The EKF algorithm can be given by the following equations:

$$P_{k+1|k} = F_K P_k {F_K}^T + Q \tag{44}$$

$$K_K = P_{k+1|k} {H_k}^T \left(H_k P_{k+1|k} {H_k}^T + R\right)^{-1} \tag{45}$$

$$\hat{x}_{k+1|k} = f\left(\hat{x}_{k|k}.u_k\right) \tag{46}$$

$$\hat{x}_{k+1|k+1} = \hat{x}_{k+1|k} + K_K\left(z_k - h\left(\hat{x}_{k+1|k}\right)\right) \tag{47}$$

$$P_{k+1|k+1} = (I - K_K H_k) P_{k+1|k} \tag{48}$$

where $P_{k+1|k}$ is the priori prediction error covariance matrix, $P_{k+1|k+1}$ is the posteriori prediction error covariance matrix, K_K is the Kalman gain, $\hat{x}_{k+1|k}$ is the priori state prediction vector, $\hat{x}_{k+1|k+1}$is the posteriori state prediction vector, Q and R are the covariance matrixes of process and measurement noise, I is the unit matrix symbol, and F_K and H_k are the Jacobians of the system and the measurement equations defined as follows:

$$F_K = \begin{bmatrix} \frac{\partial \dot{y}_k}{\partial \dot{y}_k} & \frac{\partial \dot{y}_k}{\partial \dot{\psi}_k} & \frac{\partial \dot{y}_k}{\partial \xi_k} & \frac{\partial \dot{y}_k}{\partial \mu_k} & \frac{\partial \dot{y}_k}{\partial F_{ak}} \\ \frac{\partial \dot{\psi}_k}{\partial \dot{y}_k} & \frac{\partial \dot{\psi}_k}{\partial \dot{\psi}_k} & \frac{\partial \dot{\psi}_k}{\partial \xi_k} & \frac{\partial \dot{\psi}_k}{\partial \mu_k} & \frac{\partial \dot{\psi}_k}{\partial F_{ak}} \\ \frac{\partial \xi_k}{\partial \dot{y}_k} & \frac{\partial \xi_k}{\partial \dot{\psi}_k} & \frac{\partial \xi_k}{\partial \xi_k} & \frac{\partial \xi_k}{\partial \mu_k} & \frac{\partial \xi_k}{\partial F_{ak}} \\ \frac{\partial \mu_k}{\partial \dot{y}_k} & \frac{\partial \mu_k}{\partial \dot{\psi}_k} & \frac{\partial \mu_k}{\partial \xi_k} & \frac{\partial \mu_k}{\partial \mu_k} & \frac{\partial \mu_k}{\partial F_{ak}} \\ \frac{\partial F_{ak}}{\partial \dot{y}_k} & \frac{\partial F_{ak}}{\partial \dot{\psi}_k} & \frac{\partial F_{ak}}{\partial \xi_k} & \frac{\partial F_{ak}}{\partial \mu_k} & \frac{\partial F_{ak}}{\partial F_{ak}} \end{bmatrix} \tag{49}$$

$$H_k = \begin{bmatrix} \frac{\partial \ddot{y}_k}{\partial \dot{y}_k} & \frac{\partial \ddot{y}_k}{\partial \dot{\psi}_k} & \frac{\partial \ddot{y}_k}{\partial \xi_k} & \frac{\partial \ddot{y}_k}{\partial \mu_k} & \frac{\partial \ddot{y}_k}{\partial F_{ak}} \\ \frac{\partial \dot{\psi}_k}{\partial \dot{y}_k} & \frac{\partial \dot{\psi}_k}{\partial \dot{\psi}_k} & \frac{\partial \dot{\psi}_k}{\partial \xi_k} & \frac{\partial \dot{\psi}_k}{\partial \mu_k} & \frac{\partial \dot{\psi}_k}{\partial F_{ak}} \end{bmatrix} \tag{50}$$

The Jacobian matrices mentioned in (49) and (50) are used to specify the process and measurement matrices, which are shown in (51) and (52) respectively.

$$F_k = \begin{bmatrix} 1 - a_{11} & 0 & -\frac{F_{ak-1}}{\xi_{k-1}} a_{13} & 0 & a_{13} \\ 0 & 1 - \frac{m_w S^2}{J_w} a_{11} & \frac{F_{ak-1}}{\xi_{k-1}} a_{23} & 0 & -a_{23} \\ -\frac{m_w}{2\tau V} a_{13} & \frac{J_w}{2\tau V} a_{23} & 0 & 0 & 0 \\ 0 & 0 & a_{43} & 0 & 0 \\ 0 & 0 & a_{53} & a_{54} & 0 \end{bmatrix} \tag{51}$$

in which matrix elements are as follows:

$$a_{11} = \frac{2\tau F_{ak-1}}{\xi_{k-1} m_w V}$$

$$a_{13} = -\frac{2\tau}{\xi_{k-1} m_w}\left[\frac{\dot{y}_{k-1}}{V} - \psi\right]$$

$$a_{23} = \frac{2\tau S}{\xi_{k-1} J_w}\left[\frac{\kappa_w (y - y_d)}{r} + \frac{S\dot{\psi}_{k-1}}{V}\right]$$

$$a_{43} = -BV\mu_0\left((1-D)e^{-B\xi_{k-1}V}\right.$$

$$a_{53} = \frac{4a^2 bc}{3}\left(\frac{k_A\left(1-(k_A\varepsilon)^2\right)}{\left(1+(k_A\varepsilon)^2\right)^2} + \frac{k_S}{1+(k_S\varepsilon)^2}\right)$$

$$a_{54} = \left(k_A \frac{F_N \varepsilon}{\pi}\right)^3 \left(\frac{2\pi}{F_N\left(1+(k_A\varepsilon)^2\right)}\right)^2 + \frac{2F_N}{\pi} arctg k_s \varepsilon - \frac{2k_S F_N \varepsilon}{\pi\left(1+(k_S\varepsilon)^2\right)}$$

$$H_k = \begin{bmatrix} -\frac{1}{\tau} a_{11} & 0 & -\frac{F_{ak-1}}{\tau \xi_{k-1}} a_{13} & 0 & \frac{1}{\tau} a_{13} \\ 0 & 1 - \frac{m_w S^2}{J_w} a_{11} & \frac{F_{ak-1}}{\xi_{k-1}} a_{23} & 0 & -a_{23} \end{bmatrix} \tag{52}$$

In estimating adhesion based on longitudinal, lateral and yaw dynamics, the measurement matrix includes lateral acceleration and yaw rate. In addition, inertial sensors are used to measure lateral acceleration and yaw rate.

Finally, the outputs obtained from the measurements of the sensors (accelerometer and gyroscope) and the predicted measurements are used to estimate the states. Fig. 4 shows the process.

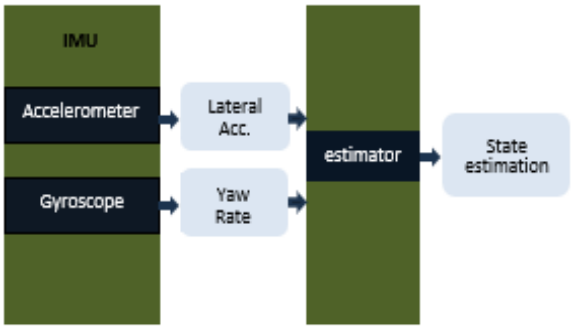

Fig. 4: State estimation overview.

Typically, the extended Kalman filter is not considered to be an optimal estimator and still has some shortcomings such as:

(1) Utilizing with the highly nonlinear system can be quite challenging.
(2) Since it needs Jacobian matrices for linearization, analytical derivation of this matrices is difficult and numerical derivation may impose a higher computational cost.
(3) The linearization introduces approximation errors that are not accounted for in the prediction and update steps.
(4) Due to the uncertainty surrounding the values of Q and R, they are acquired through trial-and-error approaches, resulting in a laborious and time-consuming process.

Referring to the EKF deficiencies, it is necessary to use an estimator that does not have such drawbacks in the estimation process. In the following, alternative estimators are investigated and their performances are compared.

B. Unscented Kalman Filter

The UKF is an alternative approach to linearization. While EKF treats the nonlinearity using analytical linearization, the UKF performs statistical linearization based on a set of rules. The approximation errors are consequences of linearization, which lead the EKF to underestimate state uncertainties. The UKF is formulated through the integration of the unscented transformation (UT) method, which is for calculating the statistics of a random variable that undergoes a nonlinear transformation. It is assumed that the wheelset system is in discrete-time nonlinear form with the state vector $\hat{x}_k$, the input vector u_k, and the observation vector z_k.

$$x_{k+1} = f(\hat{x}_k, u_k) + w_k \qquad w_k \sim (0, Q_k) \tag{53}$$

$$z_k = h(\hat{x}_k, u_k) + v_k \quad v_k \sim (0, R_k) \tag{54}$$

where Q and R are the system and observation noise covariance respectively.

At the beginning of the UKF implementation to estimate the state variables of the wheelset, a set of $2n_x + 1$ weighted samples or sigma points are determined as follows:

$$\chi_{k|k}^0 = \hat{x}_{k|k} \qquad i = 0 \tag{55}$$

$$\chi_{k|k} = \hat{x}_{k|k} + \left(\sqrt{(n_x + \lambda)P_{k|k}}\right)_i \qquad i = 1, \dots, n_x$$
$$\chi_{k|k} = \hat{x}_{k|k} - \left(\sqrt{(n_x + \lambda)P_{k|k}}\right)_i \qquad i = n_x + 1, \dots, 2n_x$$

$$w_m^{(0)} = \frac{\lambda}{\lambda + n_x} \tag{56}$$

$$w_c^{(0)} = \frac{\lambda}{\lambda + n_x} + 1 - \alpha^2 + \beta \tag{57}$$

$$w_c^{(i)} = w_m^{(i)} = \frac{\lambda}{2(\lambda + n_x)} \qquad i = 1, \dots, 2n_x \tag{58}$$

where $\hat{x}_{k|k}$ is the mean of x_{k+1}, $(\sqrt{(n_x + \lambda)P_{k|k}})_i$ is the ith-column of the matrix square root, $P_{k|k}$ is the covariance of x_{k+1}, n_x is the dimension of the state variables. The weights w_m and w_c are utilized for determining the mean and covariance respectively. α is employed to regulate the distribution of the sigma points around $\hat{x}_{k|k}$ and usually set to a small positive value between 0 and 1. β is a non-negative term utilized to incorporate prior knowledge of the distribution of x_{k+1}. Finally, $\lambda = \alpha^2(n_x + \rho) - n_x$ is a scaling parameter in which ρ is a secondary scaling parameter usually set to 0. It should be noted that in this study, the mentioned parameters are set as follows:

$$\alpha = 1, \quad \beta = 0, \quad \rho = 1$$

Sigma points $\chi_{k|k}$ are propagated through the nonlinear equations of the wheelset system. The transformed sigma points are assessed for each of the 0 to $2n_x$ points in the manner outlined below:

$$\chi_{k+1|k}^{(i)} = f(\chi_{k|k}^{(i)}, u_k) \tag{59}$$

The mean and covariance of the priori state estimation at time k are obtained by the following equations:

$$\hat{x}_{k+1|k} = \sum_{i=0}^{2n_x} w_m^{(i)} \chi_{k+1|k}^{(i)} \tag{60}$$

$$P_{k+1|k} = \sum_{i=0}^{2n_x} w_c^{(i)} (\chi_{k+1|k}^{(i)} - \hat{x}_{k+1|k})(\chi_{k+1|k}^{(i)} - \hat{x}_{k+1|k})^T + Q_k \tag{61}$$

In order to implement the measurement update, the equations (62)-(69) will be utilized. The transformed sigma points can be utilized to predict the measurements through the known nonlinear measurement equation. After rearranging the weighted sigma points, the covariance of the predicted measurement can be estimated. To consider the measurement noise, the covariance matrix R_k should be incorporated. Following that, the cross covariance can be estimated as per equation (65).

$$\chi_{k|k}^{(i)} = \left[\hat{x}_{k|k}^{(i)} \quad \hat{x}_{k|k}^{(i)} \pm \left(\sqrt{(n_x + \lambda)P_{k|k}^{(i)}}\right)_i\right] \tag{62}$$

$$\xi_{k+1|k}^{(i)} = h_{k+1}(\chi_{k+1|k}^{(i)}, U_{k+1}) \tag{63}$$

The expected measurement $\hat{z}_{k+1|k}$ is as:

$$\hat{z}_{k+1|k} = \sum_{i=0}^{2n_x} w_m^{(i)} \xi_{k+1|k}^{(i)} \tag{64}$$

Using the predicted sigma points, $P^{xz}_{k+1|k}$and $P^{zz}_{k+1|k}$ also determines as follows:

$$P^{zz}_{k+1|k} = \sum_{i=0}^{2n} \omega_i^{(c)} (\xi^{(i)}_{k+1|k} - \hat{z}_{k+1|k})(\xi^{(i)}_{k+1|k} - \hat{z}_{k+1|k})^T + R_k \quad (65)$$

$$P^{xz}_{k+1|k} = \sum_{i=0}^{2n} \omega_i^{(c)} (\chi^{(i)}_{k+1|k} - \hat{x}_{k+1|k})(\xi^{(i)}_{k+1|k} - \hat{z}_{k+1|k})^T \quad (66)$$

The mean and square root of covariance for the states are recalculated based on the actual measurement.

$$\hat{x}_{k+1|k+1} = \hat{x}_{k+1|k} + K_{k+1}(z_{k+1} - \hat{z}_{k+1|k}) \quad (67)$$

$$P_{k+1|k+1} = P_{k+1|k} - K_{K+1} P^{zz}_{k+1|k} K^T_{k+1} \quad (68)$$

$$K_{k+1} = P^{xz}_{k+1|k} (P^{zz}_{k+1|k})^{-1} \quad (69)$$

From the above equations shown for UKF, it can be concluded that this filter has two main advantages compared to EKF, firstly, there is no need for Jacobians in UKF implementation, and secondly, UKF can estimate the mean and covariance of the states accurately the second order for any nonlinearity.

Results

In this part, wheel and rail adhesion force is estimated based on the lateral, longitudinal, and yaw dynamics of the wheelset. The values of the parameters mentioned in the equations of the previous sections are given in Table 1 and Table 2. It is worth noting that all simulations are done in MATLAB environment.

Table 1: Polach model parameters under different friction condition

Model parameter	Wheel–rail conditions			
	Dry	Wet	Low	Very Low
k_A	1	1	1	1
k_S	0.4	0.4	0.4	0.4
D	0.6	0.2	0.2	0.1
B	0.4	0.4	0.4	0.4

Table 2: Parameter values used in the simulation

$K_s(\frac{N}{m})$	6063260	$K_w\ (\frac{N}{rad})$	5×10^6
$r\ (m)$	0.5	$S(m)$	0.75
$J_R(Kgm^2)$	134	$\kappa_w\ (rad)$	0.15
$J_L(Kgm^2)$	64	$M_t\ (Kg)$	15000
$J_w(Kgm^2)$	700	FN (KN)	60
$m_w\ (Kg)$	1250	G $(\frac{N}{m^2})$	8.4×10^{10}

The values of friction coefficients and other required parameters used in equations are as follows:

$$\mu_0 = \begin{cases} 0.55 & t < 10 \\ 0.3 & 10 \le t < 20 \\ 0.06 & 20 \le t < 30 \\ 0.03 & 30 \le t < 35 \end{cases}$$

a = 0.0015 m, b = 0.0075 m, C_{11} =4.12, V= 15 $\frac{m}{s}$

Matrices Q and R are as follows:

Q = diag([5× 10^{-14},1× 10^{-14},1× 10^{-14},1 × 10^{-14} , 1× 10^{-14}])

R= diag([1× 10^{-1}, 1× 10^{-1}])

At the beginning of the simulation, Fig. 5 is developed based on the equations (11)-(17). In addition, a random input y_d is created to simulate the dynamics of the wheelset in the presence of irregularities that can be encountered in the railroad. In this model, the dynamics of each wheel in the right and left sides are shown separately.

Finally, the output of right and left wheel blocks attached to the lateral acceleration and yaw rate blocks. The main goal of developing this simulink model is to simulate the outputs of accelerometer and gyroscope sensors. In estimation process these outputs along with the predicted variables of the same type are used to estimate the state variables. Figs. 6 and 7 show the results of measuring lateral acceleration and yaw rate, respectively which are obtained from simulink execution.

In Fig. 8 the diagrams of lateral speed, yaw rate, slip, adhesion coefficient, and adhesion force of the wheelset are shown. These outputs show the simulation of the actual conditions of the system. In the estimator evaluation stage, the trajectories of these graphs are used as a pattern and the estimator's compliance in following the relevant pattern is used as a criterion to check the accuracy of the estimator in the estimation of state variables.

In Figs. 9-13 the diagrams of yaw rate, lateral speed, slip ratio, adhesion coefficient and adhesion force of the wheelset are shown in three situations, UKF-baesd and EKF-based estimated, and actual.

In Fig. 9, the actual and estimated trajectories of yaw rate change approximately between 0.8 and -0.8 and from the beginning the convergence of the estimated trajectories to the actual one is evident.

In Fig. 10, the actual and estimated trajectories of lateral velocity are depicted. As can be seen, the UKF-based estimated lateral velocity converges to the actual one in less than 1 second but this convergence in EKF-based estimation occurs after 5 seconds.

Therefore, the UKF estimator has provided an acceptable results regarding these two variables. In Figs. 11-13 which are related to the slip, adhesion coefficient and adhesion force respectively, the outputs of the two estimators are drawn and compared with real variables of the same type.

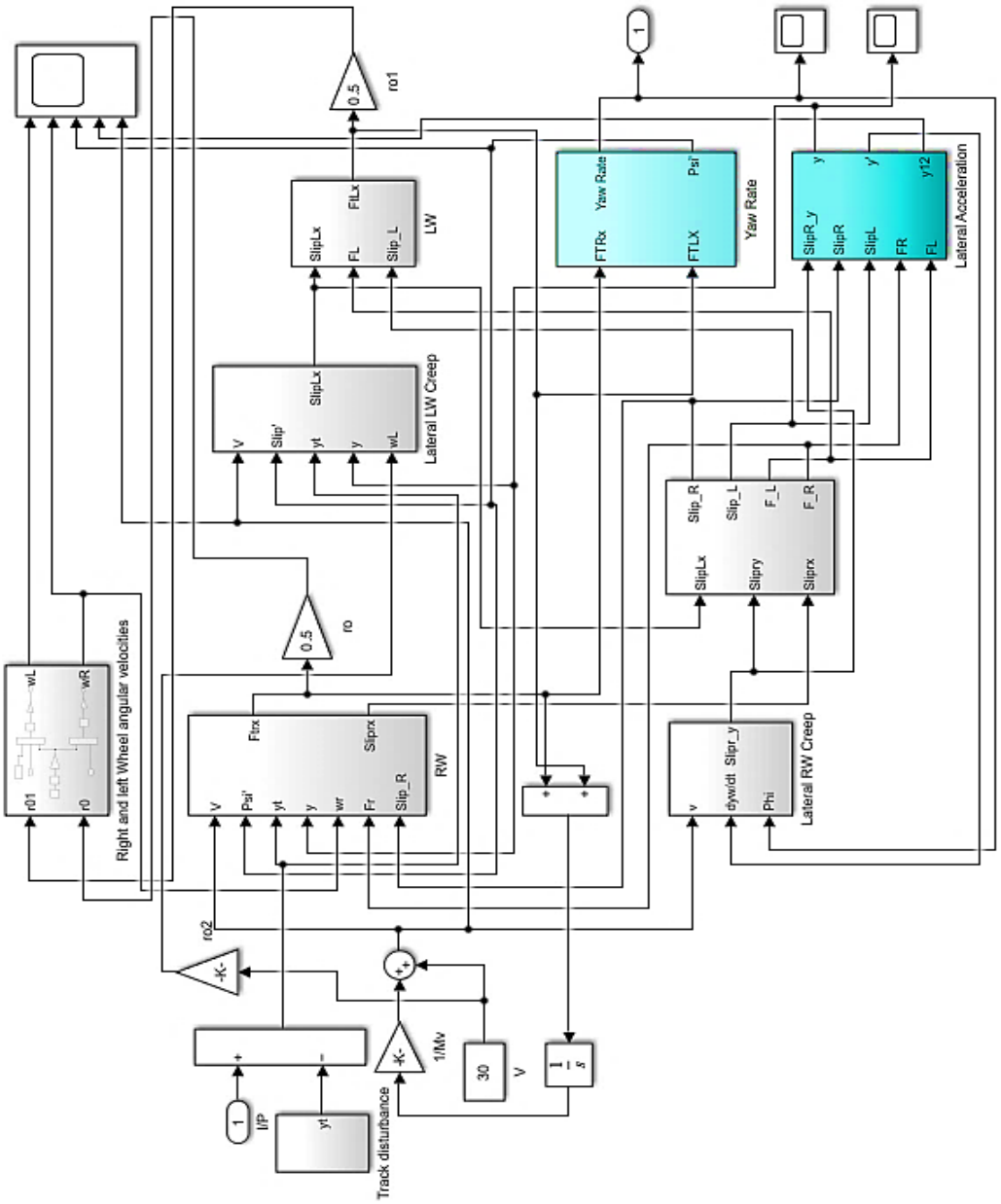

Fig. 5: Wheelset dynamics simulink model.

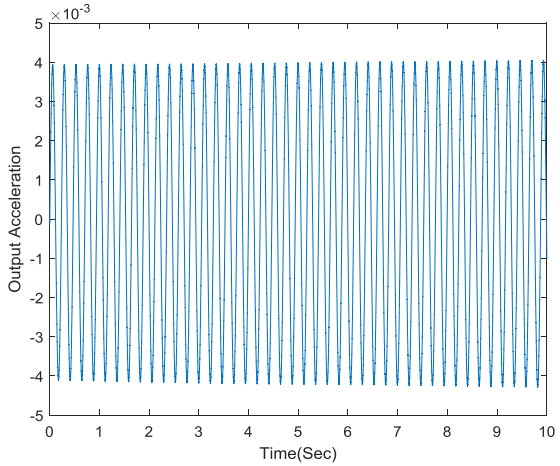

Fig. 6: Output diagram of accelerometer.

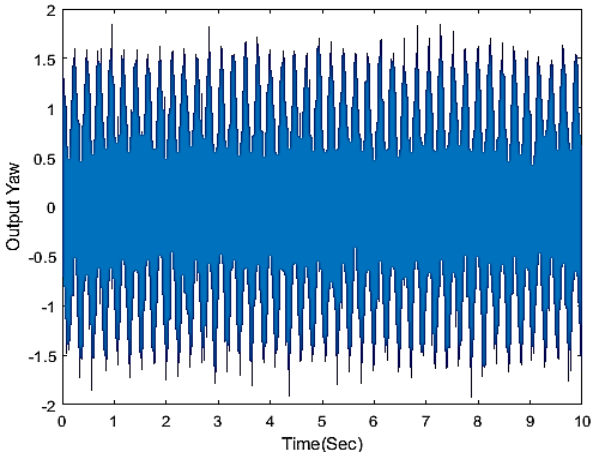

Fig. 7: Output diagram of gyroscope.

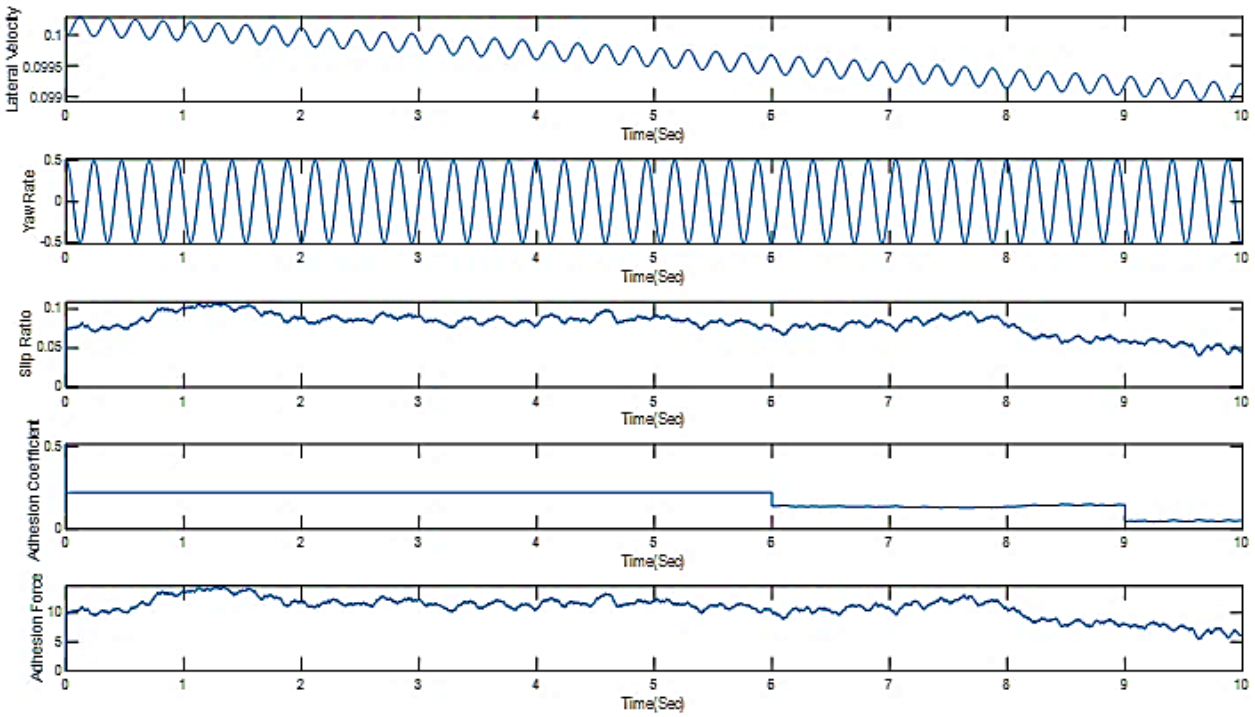

Fig. 8: dynamics of the wheelset.

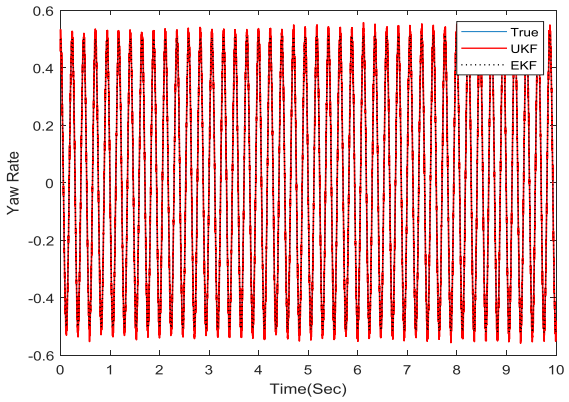

Fig. 9: Estimated, and actual trajectories of yaw rate.

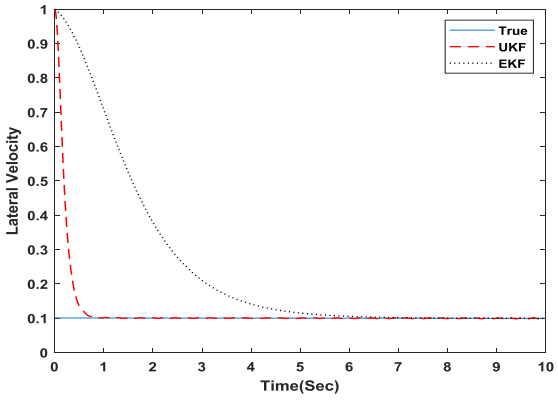

Fig. 10: Estimated, and actual trajectories of lateral velocity.

In Figs. 11-13 the simulation is carried out for 10 seconds to calculate slip ratio, adhesion coefficient, and adhesion force. All mentioned variables are estimated by EKF and UKF estimators.

Due to the irregularities exist in the lateral direction, fluctuations in the graphs are inevitable.

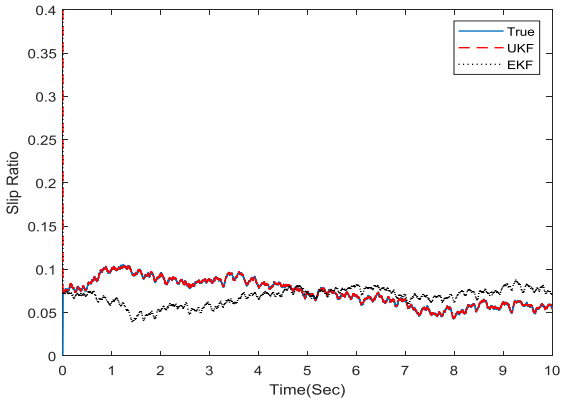

Fig. 11: Estimated, and actual trajectories of slip.

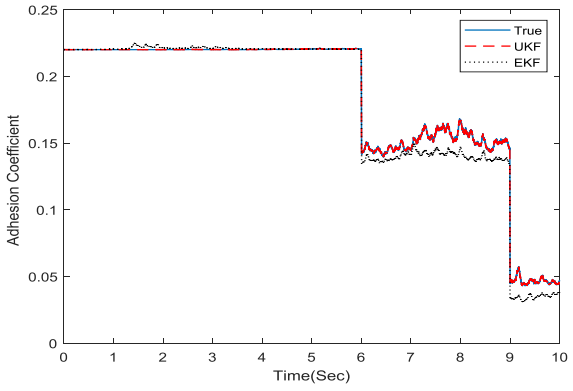

Fig. 12: Estimated and actual trajectories of adhesion coefficient.

In all three figures, UKF-based estimated outputs follow the actual trajectories of the variables with high convergence and accuracy but there is no necessary

convergence in the estimation of the mentioned variables based on EKF, which is more evident in estimating slip ratio and adhesion force. As can be seen in Fig. 12, estimation of adhesion coefficient with EKF has acceptable output up to 6 second but non-convergence after 6 second leads to ignoring this estimator as an ideal one. Therefore, in addition to the successful performance in estimating lateral velocity and yaw rate, UKF also shows a favorable performance in estimating slip ratio, adhesion coefficient, and adhesion force.

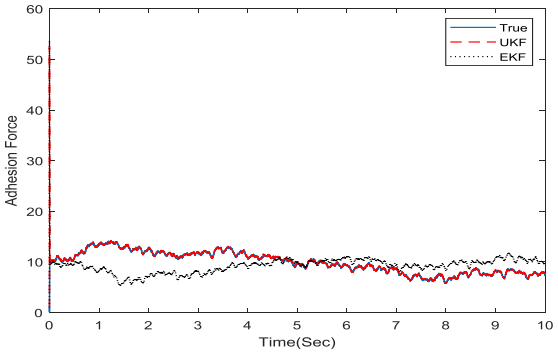

Fig. 13: Estimated and actual trajectories of adhesion force.

Conclusion and Future Work

The performance of railway operation mainly is affected by wheel-rail contact forces but it is not possible to measure these contact forces and interrelated dynamics directly, therefore it is necessary to estimate these wheelset dynamics through state of art technique. In this research paper, a railway wheelset model and a novel observer-based estimator are developed in Simulink/MATLAB to calculate and estimate nonlinear wheelset dynamics. The estimators based on the EKF and UKF are used to estimate adhesion coefficient, slip ratio, and yaw rate effectively in dry, wet, greasy and extremely slippery track conditions. The performances of the UKF and EKF algorithms are assessed and compared with each other. The UKF estimator not only verified excellent performance in the normal operation of a railway vehicle on a normal track but equally depicted robustness in traction and braking modes of the vehicle in wet, oily, and extremely slippery track conditions. The validity of the estimator is also checked in the transition of adhesion conditions from dry to extremely slippery and vice-versa during the simulation. In the future, this approach will be implemented on Field Programmable Gate Arrays (FPGA) platform for real-time condition monitoring of wheelset dynamics to avoid the accidents and derailment of railway vehicle.

Author Contributions

M. Moradi collected the data, carried out the analysis and wrote paper, R. Havangi wrote the paper, interpreted the results and supervised the research.

Acknowledgment

This work is completely self-supporting, thereby no any financial agency's role is available.

Conflict of Interest

The authors declare no potential conflict of interest regarding the publication of this work. In addition, the ethical issues including plagiarism, informed consent, misconduct, data fabrication and, or falsification, double publication and, or submission, and redundancy have been completely witnessed by the authors.

Abbreviations

a and b	Semi-axis length of the contact patch
B and D	Reduction factors
c	Contact shear stiffness coefficient
F_c	Centrifugal force
F_N	Normal force between the wheel and rail
k_A	Reduction factor in the adhesion area
k_S	Reduction factor in the slip area
M_t	Rail vehicle mass
n_i	Gear reduction ratio
r	Wheel radius
R_r and R_s	Rotor and stator resistance
S	Half gauge of track
T_m	Motor torque
T_L	Load torque
V	Longitudinal velocity
V_{wR}	Longitudinal velocity of the right wheel
V_{wL}	Longitudinal velocity of the left wheel
y	Lateral movement
y_d	Track irregularities in lateral direction
ϵ	Gradient of tangential stress
κ_w	Wheel conicity
ψ	Yaw angle
ξ	Total creepage between the wheel and rail
ξ_x	Longitudinal creepge
ξ_y	Lateral creepage
μ_f	Friction coefficient
μ_0	Maximum friction coefficient
ω_R	Angular velocity of the right wheel
ω_L	Angular velocity of the left wheel

References

[1] E. E. Magel, "A survey of wheel/rail friction," (No. DOT/FRA/ORD - 17-21), Federal Railroad Administration. Office of Research, Development, and Technology, Washington, DC, United States, 2017.

[2] U. Olofsson, "17 Adhesion and friction modification," in Wheel–Rail Interface Handbook, ELSEVIER, UK, pp. 510-527, 2009.

[3] Z. Yuan, M. Wu, C. Tian, J. Zhou, "A review on the application of friction models in wheel-rail adhesion calculation," Urban Rail Transit, 7: 1-11, 2021.

[4] Z. Shi, K. Wang, L. Guo, Z. Chen, "Effect of arc surfaces friction coefficient on coupler stability in heavy haul locomotives: simulation and experiment," Veh. Syst. Dyn., 55(9): 1368-1383, 2017.

[5] L. Buckley-Johnstone, G. Trummer, P. Voltr, K. Six, R. Lewis "Full scale testing of low adhesion effects with small amounts of water in the wheel/rail interface," Tribol. Int., 141: 105907, 2020.

[6] R. Lewis, G. Trummer, K. Six, J. Stow et al., "Leaves on the line: characterising leaf based low adhesion on railway rails," Tribol. Int., 185: 108529, 2023.

[7] H. Chen, "Wheel slip/slide and low adhesion caused by fallen leaves," Wear, 203187: 446-447, 2020.

[8] J. Zhou, M. Wu, C. Tian, Z. Yuan, C. Chen, "Experimental investigation on wheel–rail adhesion characteristics under water and large sliding conditions," Ind. Lubr. Tribol., 73(2): 366-372, 2021.

[9] K. Zhao, P. Li, Ch. Zhang, J. He, Y. Li, T. Yin, "Online accurate estimation of the wheel-rail adhesion coefficient and optimal adhesion antiskid control of heavy-haul electric locomotives based on asymmetric barrier lyapunov function," J. Sensors, 2740679: 1-12, 2018.

[10] R. Bibi, B. S. Chowdry, R. A. Shah, "PSO based localization of multiple mobile robots employing LEGO EV3," in Proc. 2018 International Conference on Computing, Mathematics and Engineering Technologies (iCoMET): 1-5, 2018.

[11] K. Ishizaka, B. White, M. Watson, S. R. Lewis, R. Lewis, "Influence of temperature on adhesion coefficient and bonding strength of leaf films: a twin disc study, Wear, 203330: 454-455, 2020.

[12] S. Shrestha, Q. Wu, M. Spiryagin, "Review of adhesion estimation approaches for rail vehicles," Int. J. Rail Transp., 7(2): 79-102, 2019.

[13] X. Fang, S. Lin, Z. Yang, F. Lin, H. Sun, L. Hu, "Adhesion control strategy based on the wheel-rail adhesion state observation for high-speed trains," Electronics, 7(5): 70, 2018.

[14] B. Liu, T.X. Mei, S. Bruni, "Design and optimisation of wheel–rail profiles for adhesion improvement," Veh. Sys. Dyn., 54(3): 429-444, 2016.

[15] Y. Chen, H. Dong, J. Lu, X. Sun, L. Guo, "A super-twisting-like algorithm and Its application to train operation control with optimal utilization of adhesion force," IEEE Trans. Intell. Transp. Syst., 17(11): 3035-3044, 2016.

[16] M. Yamashita, T. Soeda, "Anti-slip re-adhesion control method for increasing the tractive force of locomotives through the early detection of wheel slip convergence," in Proc. 17th European Conference on Power Electronics and Applications: 1-10, 2015.

[17] P. D. Hubbard, C. Ward, R. Dixon, R. Goodall, "Verification of model based adhesion estimation in the wheel-rail interface," Chem. Eng. Trans., 33: 757-762, 2013.

[18] C. P. Ward, R. M. Goodall, R. Dixon, G. A. Charles, "Adhesion estimation at the wheel–rail interface using advanced model-based filtering," Veh. Syst. Dyn., 50: 1797-1816, 2012.

[19] S. Strano, M. Terzo, "On the real-time estimation of the wheel-rail contact force by means of a new nonlinear estimator design model," Mech. Syst. Signal Process., 105: 391-403, 2018.

[20] Y. Zhao, B. Liang, "Re-adhesion control for a railway single wheelset test rig based on the behaviour of the traction motor," Veh. Syst. Dyn., 51(8): 1173-1185, 2013.

[21] S. Wang, J. Xiao, J. Huang, H. Sheng, "Locomotive wheel slip detection based on multi-rate state identification of motor load torque," J. Franklin Inst., 353(2): 521-540, 2016.

[22] P. Pichlik, J. Zdenek, "Extended Kalman filter utilization for a railway traction vehicle slip control," in Proc. International Conference on Optimization of Electrical and Electronic Equipment (OPTIM), Intl Aegean Conference on Electrical Machines and Power Electronics (ACEMP): 869-874, 2017.

[23] S. Strano, M. Terzo, "On the real-time estimation of the wheel-rail contact force by means of a new nonlinear estimator design model," Mech. Syst. Signal Process., 105: 391-403, 2018.

[24] S. J. Julier, J. K. Uhlmann, "Unscented filtering and nonlinear estimation," Proc. IEEE, 92: 401-422, 2004.

[25] S. J. Julier, J. K. Uhlmann, H. F. Durrant-Whyte, "A new approach for filtering nonlinear systems," in Proc. American Control Conference - ACC'95, Autom Control Council: 1628-1632, 1995.

[26] Y. Zhao, B. Liang, S. Iwnicki, "Friction coefficient estimation using an unscented Kalman filter," Int. J. Veh. Mech. Mobility, 52(1): 220-234, 2014.

[27] T. Gajdar, I. Rudas, Y. Suda, "Neural network based estimation of friction coefficient of wheel and rail," in Proc. IEEE International Conference on Intelligent Engineering Systems: 315-318, 1997.

[28] A. Shebani, S. Iwnicki, "Prediction of wheel and rail wear under different contact conditions using artificial neural networks," Wear, 406-407: 173-184, 2018.

[29] S. Z. Meymand, A. Keylin, M. Ahmadian, "A survey of wheel–rail contact models for rail vehicles," Int. J. Veh. Mech. Mobility, 54: 386-428, 2016.

[30] J. Belanger, P. Venne, J. N. Paquin, "The what, where and why of real-time simulation," Transient Analysis of Power Systems: Solution Techniques, Tools, and Applications, 37-49, 2011.

[31] O. Polach, "Creep forces in simulations of traction vehicles running on adhesion limit," Wear, 258: 992-1000, 2005.

[32] G. Charles, R. Goodall, R. Dixon, "Model-based condition monitoring at the wheel-rail interface," Veh. Syst. Dyn., 46: 415-430, 2008.

Biographies

Maryam Moradi received her M.S. degrees in Telecommunications Engineering from the Faculty of Engineering, University of Sistan and Baluchestan, Zahedan, Iran, in 2015, and received her Ph.D. degree in Control Engineering in Faculty of Engineering, University of Birjand, Birjand, Iran, in 2024. In 2019, she joined University of Applied Sciences & Technology as a Teacher. Her research interests are neural network, estimation and filtering.

- Email: m_moradi@birjand.ac.ir
- ORCID: 0009-0007-0635-6867
- Web of Science Researcher ID: NA
- Scopus Author ID: NA
- Homepage: NA

Ramazan Havangi received his M.S. and Ph.D. degrees from the K.N. Toosi University of Technology, Tehran, Iran, in 2003 and 2012, respectively. He is currently an Associate Professor of control systems with the Department of Electrical and Computer Engineering, University of Birjand, Birjand, Iran. His main research interests are inertial navigation, integrated navigation, estimation and filtering, evolutionary filtering, simultaneous localization and mapping, fuzzy, neural network, and soft computing.

- Email: Havangi@Birjand.ac.ir
- ORCID: 0000-0001-5711-3127
- Web of Science Researcher ID: NA
- Scopus Author ID: NA
- Homepage: https://cv.birjand.ac.ir/havangi/fa

How to cite this paper:
M. Moradi, R. Havangi, "Nonlinear filter-based estimation of wheel-rail contact forces and related considerations using inertial measurement unit," J. Electr. Comput. Eng. Innovations, 13(2): 353-364, 2025.

DOI: 10.22061/jecei.2025.11176.772

URL: https://jecei.sru.ac.ir/article_2260.html